

A Graphene Surface Force Balance

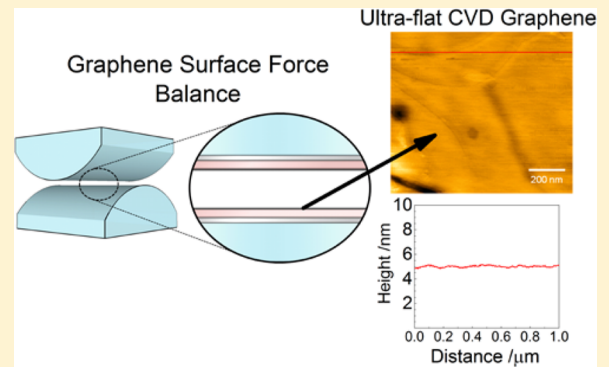
Jude Britton,^{†,‡} Nico E. A. Cousens,^{†,§} Samuel W. Coles,[§] Christian D. van Engers,[‡] Vitaliy Babenko,[‡] Adrian T. Murdock,[‡] Antal Koós,[‡] Susan Perkin,^{*,§} and Nicole Grobert^{*,‡}

[†]Department of Materials, University of Oxford, Parks Road, Oxford OX1 3PH, United Kingdom

[§]Department of Chemistry, University of Oxford, South Parks Road, Oxford OX1 3QZ, United Kingdom

Supporting Information

ABSTRACT: We report a method for transferring graphene, grown by chemical vapor deposition, which produces ultraflat graphene surfaces (root-mean-square roughness of 0.19 nm) free from polymer residues over macroscopic areas ($>1\text{ cm}^2$). The critical step in preparing such surfaces involves the use of an intermediate mica template, which itself is atomically smooth. We demonstrate the compatibility of these model surfaces with the surface force balance, opening up the possibility of measuring normal and lateral forces, including friction and adhesion, between two graphene sheets either in contact or across a liquid medium. The conductivity of the graphene surfaces allows forces to be measured while controlling the surface potential. This new apparatus, the graphene surface force balance, is expected to be of importance to the future understanding of graphene in applications from lubrication to electrochemical energy storage systems.



INTRODUCTION

Graphene is likely to play a key role in a broad range of electronic, electrochemical, and structural applications. Because the study of these systems continues to focus on the nanoscale, understanding the interaction of graphene with ultrathin films, molecular assemblies, and even individual molecules becomes increasingly important.^{1–4} To reliably investigate such structures with techniques, such as atomic force microscopy and scanning tunneling microscopy, smooth substrates, devoid of contamination and large features, are required.⁵ Similarly, surface force measurements, which require smooth surfaces over macroscopic areas, are also constrained by these requirements.⁶ Graphene can be prepared directly from graphite, either mechanically⁷ or via chemical exfoliation;⁸ however, the characteristics of the graphene flakes produced are largely uncontrollable, and the mean flake size is limited to only a few micrometers. Conversely, graphene synthesized by chemical vapor deposition (CVD) provides much larger surface areas with control over the number of graphene layers (Vlassiouk et al. report growth on 40 in. copper foils⁹). Nonetheless, difficulties arise in transferring graphene from the growth substrate to the target material, with polymer contamination of the graphene surface common when using current transfer methods.^{10–15} Furthermore, graphene is generally wrinkled because of a difference in thermal expansion coefficients of graphene and the growth substrate upon cooling after synthesis.^{16,17}

Here, we present a new and facile method of transferring CVD graphene to produce clean, molecularly smooth surfaces on the order of 1 cm^2 in area. This is made possible by a

“double-transfer” procedure, where an intermediate step uses freshly cleaved and atomically smooth mica as a template to flatten the graphene. Mica is a naturally occurring mineral, which can be cleaved to reveal a perfectly clean and flat surface over macroscopic areas, making it ideal for this process. For SFB applications, it is imperative that graphene exhibits a close to molecularly smooth roughness and polymer contamination is explicitly avoided. As a final step in this work, we demonstrate that the resulting graphene surfaces are indeed sufficiently smooth to allow for force measurements in a surface force balance (SFB), by presenting a proof-of-principle measurement. The modified instrument is referred to as a graphene surface force balance (gSFB). Some features of the resulting force profiles across aqueous solution are as yet unexplained, and future work in our laboratories will investigate the interaction between graphene sheets with externally applied potential.

The SFB^{18–20} [also called surface force apparatus (SFA)] has provided pioneering measurements over the past half-century of surface and colloidal forces in liquids: electrostatic surface forces,^{21–23} Lifshitz/van der Waals forces,^{18,24} solvation forces,²⁵ forces because of adsorbed and grafted polymers,^{26,27} and forces because of surfactants/lipids and biological molecules²⁸ were all first characterized using this technique. The power of the method arises from the molecular (often sub-molecular) resolution in separation between two identical and atomically smooth mica sheets of precisely known contact

Received: July 18, 2014

Revised: August 26, 2014

Published: August 29, 2014

geometry, obtained using white-light interferometry. Key features of the SFB setup are shown in Figure 1. Although a

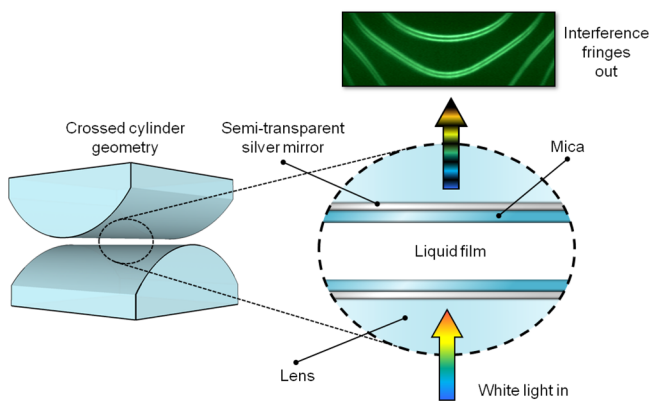


Figure 1. Schematic of the conventional mica SFB illustrating the crossed-cylinder geometry of the mica-covered lenses. Semi-transparent silver mirrors behind the mica form a white light interferometer, which is used to measure the surface separation with sub-nanometer precision. Forces at the mica surface are simultaneously measured by recording the deflection of a spring as the surfaces are brought together.

number of modifications have been made to explore different substrate materials, including the hugely desirable move to use conducting materials, it has not been possible to replace both surfaces with conducting layers of (sub)molecular roughness over the square-centimeter-sized areas as required.^{6,29–31} The difficulty arises from the simultaneous need for optical transparency, good conductivity, and molecular-scale smoothness over macroscopic ($\sim\text{cm}^2$) areas. It is the aim of this work to provide such surfaces using CVD graphene and demonstrate their potential for future surface force measurements.

In summary, we propose a new ultraflat transfer for graphene, which produces molecularly smooth, clean model surfaces. Although graphene has attracted a huge amount of attention in recent years, it has never before been used in SFB measurements. This technique facilitates a modification to the classical SFB to produce a gSFB that allows for graphene-graphene interactions to be measured across air and across liquids with simultaneous detection of their separation with sub-nanometer resolution.

MATERIALS AND METHODS

CVD Graphene Synthesis. Few-layer graphene was synthesized using atmospheric pressure chemical vapor deposition of CH_4 in the presence of H_2 on 10×25 mm Cu foils (Alfa Aesar, 99.8%, 25 μm thick). The CVD setup consisted of a quartz tube (20 mm inner diameter) located inside a horizontal cylindrical furnace and connected to an acetone bubbler. Contamination from supplier processing was removed before synthesis by sonicating copper in acetic acid for 10 min and then rinsing with deionized water.³² Copper foil was placed inside the quartz tube at 1035 °C and annealed for 30 min in the presence of 500 standard cubic centimeters per minute (scfm) H_2 to further clean the copper surface and increase the copper grain size. Hydrogen flow was then reduced to 300 scfm, and 5 scfm CH_4 was introduced for 50 min for few-layer graphene growth.

Graphene to Mica Transfer. Graphene was transferred from the copper foil by drop-coating poly(methyl methacrylate) (PMMA; molecular weight = 996 000, dissolved in chlorobenzene) onto one side of the foil and then etching the copper in 0.1 M ammonium persulfate solution. The PMMA/graphene was then removed from the etchant solution and washed thoroughly with ultrapure water [18.2

Ω resistivity, <1 ppb total organic carbon (TOC)]. It was then placed onto freshly cleaved mica, graphene side down, and pressed between glass microscope slides at 110 °C for 30 min. PMMA was removed by submerging the sample in glacial acetic acid (Fisher, extra pure) for 2 h.

Lens Preparation. A total of 40 nm of Ag (Alfa Aesar, 99.999%) was thermally evaporated under vacuum (0.3 \AA s^{-1} , 10^{-6} mbar) onto hemispherical quartz lenses (1 cm diameter, 1 cm radius of curvature). Fringes arising from silver mirrors evaporated onto quartz lenses were similar to fringes arising from back-silvered mica and smooth enough to resolve long-range forces. Alternatively, the mirrors can also be prepared via the template stripping method, which produces atomically smooth mirrors with potentially increased resolution. Buelher EpoThin epoxy diluted with ethanol (Sigma-Aldrich, >99.8%, 1:2 ratio by volume) was spin-coated onto the Ag surface with a Laurel WS650 Mz-23NPP/LITE spin coater. The following spin cycle was used: accelerate at 100 rpm s^{-1} for 5 s and then accelerate to 3000 at 300 rpm s^{-1} for 30 s.

Graphene on mica was then laid onto the surface, and the epoxy was left to cure overnight. The mica could then be removed, and the ultraflat graphene was exposed immediately prior to use in the SFB. Submerging the lens in ultrapure water facilitated removal of the mica.

SFB. The SFB used has been described in detail elsewhere;²⁰ a full paper describing the setup and operation of the modified gSFB will be communicated in due course. Essential details of the setup relating to this proof-of-principle experiment are as follows. Two hemicylindrical lenses, with graphene sheets attached as described in the text, were mounted in crossed-cylinder configuration inside the SFB. One lens was translated toward or away from the other, in the perpendicular direction, using a motor and a differential spring mechanism to achieve fine control. Forces were detected via the bending of a spring upon which one surface is mounted. Under high applied loads, the glue layer was compressed, leading to a systematic error in the separation distance under high load; this was corrected by subtraction of a linear fit to the compressive behavior from the measured data points.

The separation distance between the lenses was measured using white-light interferometry. Fringes arising from reflection between the silver layers on the lenses [“fringes of equal chromatic order” (FECO)] were observed in a grating spectrometer and captured using a charge-coupled device (CCD) camera. The shape and location of the fringes within these images were extrapolated using a method similar to that used by Quon et al.³³ In this method, each row of the pixels is fitted separately to map the fringe. However, in contrast to previous work, the algorithm here used a one-dimensional center of mass centroid fit instead of a Gaussian fit.

By approximating that the two glue layers are of the same thickness and noting that the thickness of the glue is far greater than that of graphene, the interferometer was estimated to behave as a three-layer symmetric interferometer. This allowed for the fringe locations from within the images to be converted into distance separation using the standard analytical solution for a three-layer interferometer described elsewhere.³⁴ The refractive index used for the epoxy was 1.532. The surface curvature of the graphene was calculated from the Derjaguin-Landau-Verwey-Overbeek (DLVO) fitting process and was found to be 2 cm in this case.

The potential of the graphene surfaces was controlled with a Metrohm μAutolabIII potentiostat, with Pt wire as the reference electrode, and the effective surface potential at the region of interaction was measured from the minimum point of an electrocapillary curve obtained through electrochemical impedance spectroscopy (see Figure S1 of the Supporting Information). Electrical connections to the graphene surfaces were made with silver conductive paint (RS Components). Potassium perchlorate (99.99%) from Sigma-Aldrich was used as supplied.

Sample Characterization. CVD graphene was characterized by scanning electron microscopy (SEM), Raman spectroscopy and atomic force microscopy (AFM). For SEM imaging, a JEOL JSM-6500F was operated at 5 kV. Raman spectroscopy was conducted at room temperature using a JY Horiba LabRAM Aramis Raman spectrometer equipped with a 532 nm laser. Atomic force micrographs

were recorded with a NanoScope MultiMode AFM in contact mode (Nanosensors PointProbe Plus Contact Mode probes).

RESULTS AND DISCUSSION

Outline of the Procedure (Full Details Are Provided in the Materials and Methods). We present a new five-layer interferometer setup, analogous to the traditional mica–film–mica interferometer used in SFB, consisting of epoxy–graphene–film–graphene–epoxy (where the film can be air, vapor, or a liquid), as shown in Figure 2a. The key to the

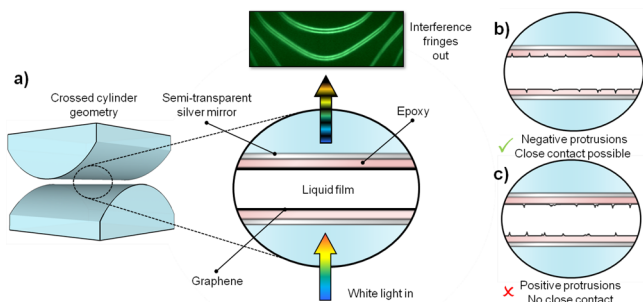


Figure 2. (a) Illustration of gSFB lens structure detailing the five-layer interferometer setup consisting of epoxy–graphene–film–graphene–epoxy. (b and c) Two sets of graphene lens surfaces showing the detrimental effect of positive protrusions on finding a contact point.

success of the graphene-coated lenses for force measurement and interferometry are (i) chemical cleanliness (e.g., absence of polymer residues from graphene transfer) and (ii) absence of “positive protrusions” in the graphene, as indicated in panels b and c of Figure 2. This was achieved by way of a new double-transfer procedure, making use of an atomically smooth and clean mica surface as a template. Individual steps in this double-transfer procedure were as follows (see the Materials and Methods for full details, and a schematic of the procedure is shown in Figure 3):

CVD Graphene Growth. Graphene was synthesized using atmospheric-pressure CVD of CH₄ in the presence of H₂ on Cu foils at 1035 °C. Gas concentrations and experimental times were tailored to synthesize high-quality, few-layer graphene. Full characterization of the graphene is described in the Graphene Characterization section.

Graphene Transfer to Mica. Graphene was transferred from the Cu foil by adapting and incorporating additional steps to a well-established conventional polymer transfer method.^{10,11} PMMA was deposited onto the graphene/Cu foil, followed by copper substrate etching. The PMMA/graphene was then removed from the etchant solution, thoroughly rinsed with ultrapure water (18.2 MΩ cm resistivity, <1 ppb total organic content), and placed onto freshly cleaved mica. The mica was cleaved such that it was thin and flexible enough to lie over a curved SFB lens. Following this, the PMMA/graphene was pressed into the mica surface at 110 °C, after which PMMA was removed with glacial acetic acid.

Graphene Transfer to Silver-Coated Lens with Necessary 2–10 μm Interferometer Thickness. To detect separation distance and interaction force, the SFB requires each of the hemicylindrical optical lenses to be covered by a partially reflective mirror, which was achieved by evaporating 40 nm of silver onto the SFB lenses. The thin silver film enables the FECO interference method to be used. Furthermore, the silver mirrors must still be separated by 2–10 μm when the graphene

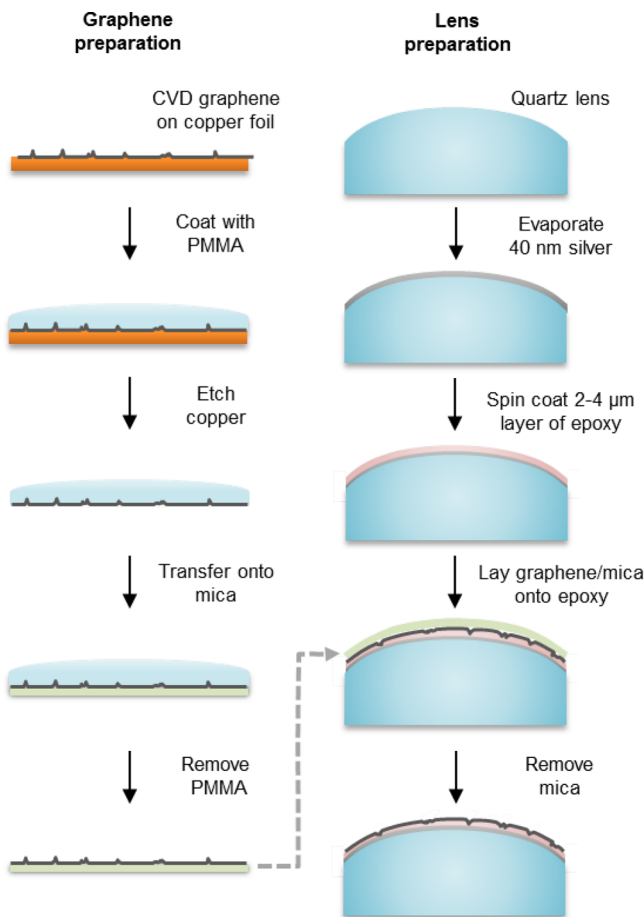


Figure 3. Schematic of graphene SFB lens fabrication. (Left) Transfer of CVD graphene onto the mica template. After CVD growth of graphene on copper, the graphene surface is coated with PMMA to provide a mechanical support for the graphene film during etching. After etching, the graphene is laid onto freshly cleaved mica. Finally, PMMA is removed with glacial acetic acid. (Right) Preparation of SFB lens with the ultraflat graphene surface suitable for the FECO interference method. A total of 40 nm of silver is evaporated onto a clean SFB lens. Subsequently, the epoxy adhesive is spin-coated onto the silver layer onto which the graphene/mica stack is placed. After curing, removal of the mica with water exposes a clean, smooth, graphene surface with no positive protrusions.

surfaces are in contact. To achieve this precise separation of the mirrors, the epoxy used to fix the graphene to the mirror was spin-coated. The resulting epoxy thickness (1–10 μm) was precisely controlled by diluting the epoxy and varying the speed and duration of the spin cycle. At this stage, the mica/graphene was laid over the epoxy-covered lenses. After the epoxy had cured, the mica was peeled off, revealing an ultraflat graphene surface, which mirrored the low roughness of the mica template. Submerging the lens in ultrapure water greatly facilitated the mica removal, presumably because of favorable interactions between water and the high-energy mica surface. The mica removal step was performed immediately prior to using the lenses in the gSFB to minimize exposure to airborne contamination and ensure that the surface was as clean as possible. For electrochemical experiments, electrical connections to the graphene sheets were made.

Graphene Characterization. CVD-synthesized graphene allows for the production of large area graphene films with precise control over the number of graphene layers.^{12,35–42}

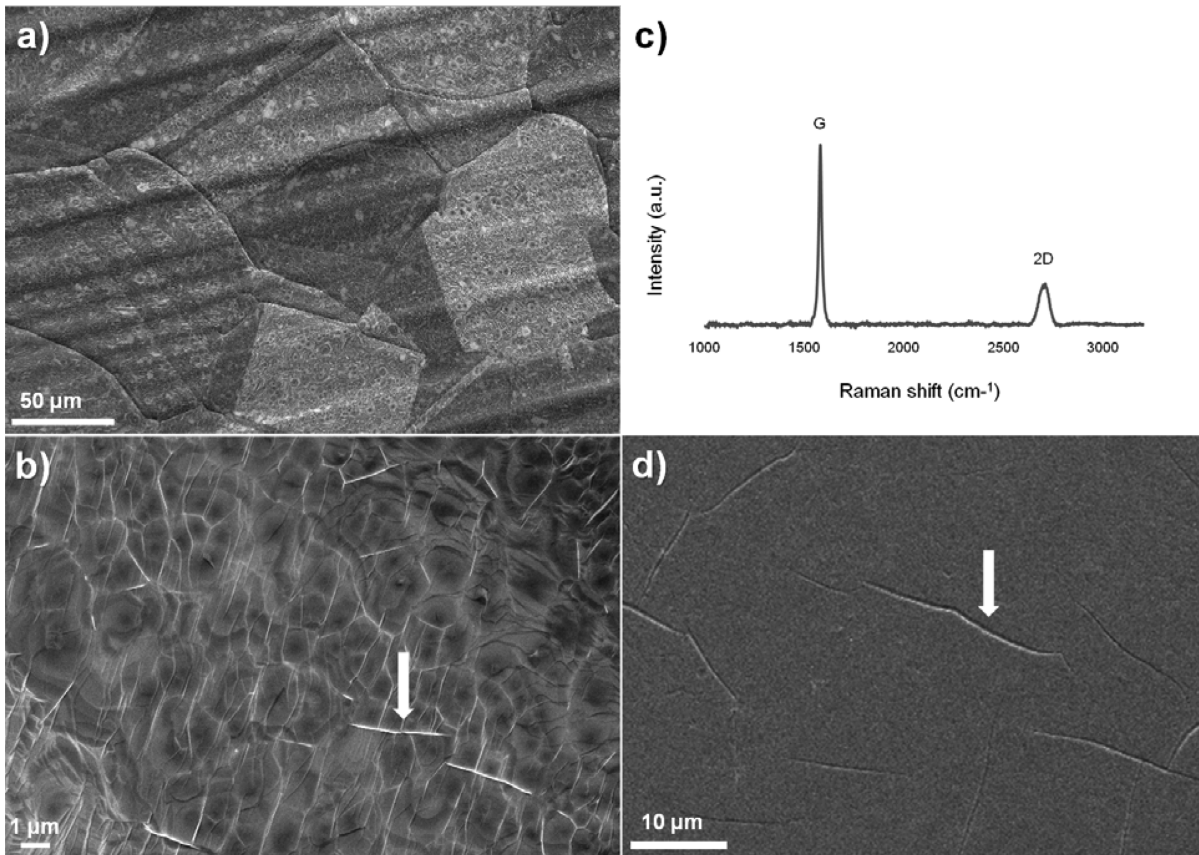


Figure 4. (a and b) SEM images of few-layer graphene (white arrow highlights an example of a wrinkle). (c) Raman spectrum of as-synthesized graphene on copper. The 2D/G ratio is characteristic of few-layer graphene. The absence of a D peak at 1350 cm^{-1} is indicative of a low-defect density. (d) SEM image of graphene transferred to a glass slide using the ultraflat technique (white arrow highlights a now inverted wrinkle, embedded in the epoxy below, as in the schematic in Figure 2b).

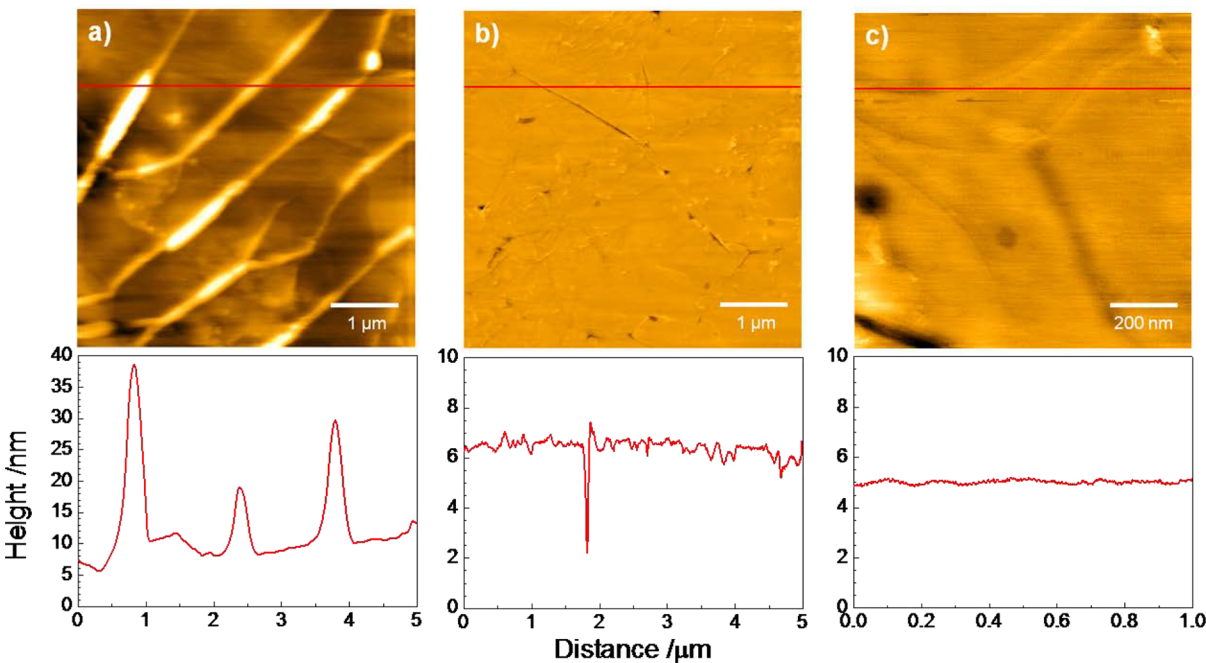


Figure 5. (Top) AFM micrographs of (a) $5\text{ }\mu\text{m}^2$ scan of the top surface of CVD graphene transferred onto mica using a conventional polymer transfer method, with 4.43 nm RMS roughness, (b) $5\text{ }\mu\text{m}^2$ scan of ultraflat CVD graphene transferred onto SFB lens using a double-transfer procedure, with 0.44 nm RMS roughness, and (c) $1\text{ }\mu\text{m}^2$ scan of ultraflat CVD graphene transferred onto SFB lens using a double-transfer procedure, with 0.19 nm RMS roughness. The dark areas in the bottom left of the scan are negative protrusions. (Bottom) Height profiles corresponding to the lines in the top images.

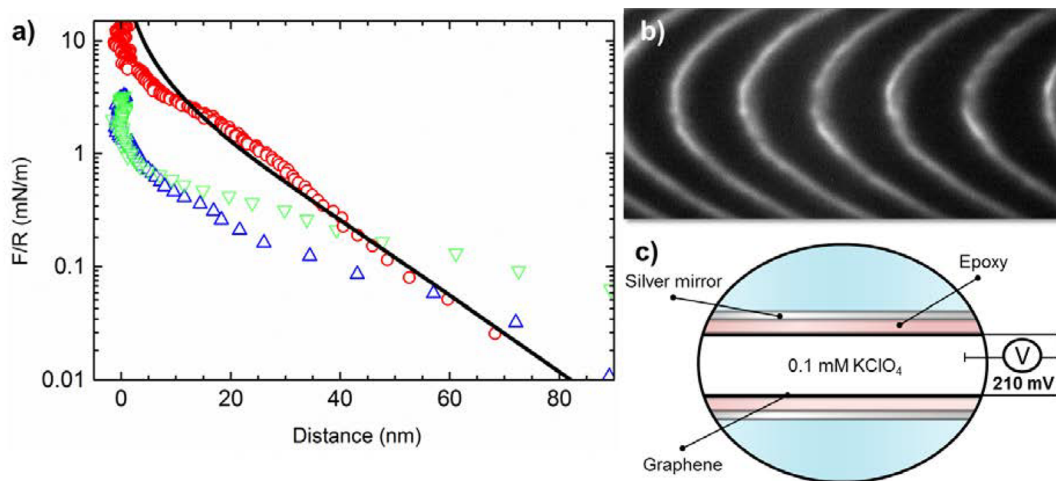


Figure 6. (a) Force–distance profile of graphene surfaces under potential control in the gSFB with 0.1 mM KClO₄ solution. Blue triangles show the system at open circuit; red circles show a −210 mV surface potential; and green triangles show the system at open circuit after the −210 mV potential had been switched off. The black line corresponds to the theoretically predicted force profile for a 0.6 mM 1:1 electrolyte solution with −210 mV surface potential. The solid green and blue lines correspond to fits for 0.1 mM 1:1 electrolyte solution. (b) Example of interference fringes used to extract the force profile. (c) Diagram of the experimental setup.

Panels a and b of Figure 4 show typical SEM images of fully covered copper substrates with few-layer (approximately 3–5) CVD graphene used in these experiments. Figure 4a demonstrates the uniform coverage of the few-layer graphene across several copper grains. As highlighted by a white arrow in Figure 4b, wrinkles were observed in these SEM images as expected for dense coverage of few-layer graphene. Regardless of this level of roughness, the proposed transfer technique still allows for molecularly smooth surfaces to be obtained.

Figure 4c shows a typical Raman spectrum of the graphene used in this study. The ratio of the 2D/G peak is indicative of few-layer graphene.^{43–45} There is no appearance of a D peak in the spectrum ($\sim 1350 \text{ cm}^{-1}$), indicating high-quality (low-defect) graphene.⁴⁶ Figure 4d shows a SEM image of graphene that was transferred onto a glass slide, as opposed to a SFB lens, via the ultraflat transfer process as outlined in Figure 3. A white arrow highlights a wrinkle that can be seen protruding into the epoxy below, as shown schematically in Figure 2c. A Raman spectrum of the graphene after transfer onto a SFB lens is shown in Figure S2 of the Supporting Information.

The resistance across the lens, measured with a two-point probe, was 0.5–2 kΩ, indicating that moderate currents (up to $\sim 1 \mu\text{A}$) could be passed through the lens without significant voltage drops or Joule heating occurring.

Full coverage of graphene across the copper foil was preferred for SFB purposes to ensure that only graphene–graphene interactions were probed rather than graphene–epoxy interactions. The benefits of few-layer graphene in SFB experiments are expected to be twofold: increased screening of intermolecular forces from the underlying epoxy and increased conductivity of the surface.⁴⁷ It has been shown that monolayer graphene is essentially “transparent” to the van der Waals forces of the underlying support material; however, as the number of graphene layers increases, the contact angle of a water droplet approaches that of water on graphite.⁴⁸

Conductivity of the surface is of interest because a conductive surface permits external control of the surface potential. The recorded resistance affirms the viability of using the gSFB for electrochemical and other potential-dependent experiments.

Roughness Analysis of Ultraflat Surfaces. Graphene surfaces were imaged with AFM. Figure 5a shows CVD graphene transferred onto mica before transfer to the lens (see the left-hand side of Figure 3 for transfer details). This image is representative of CVD graphene, which has been transferred to an arbitrary substrate, such as a silicon wafer, using the conventional polymer transfer method. The surface exhibits graphene wrinkles ca. 20 nm tall. Such a surface is unsuitable for surface force measurements because the protrusions prevent close contact of the surfaces (see Figure 2c).

When the graphene is flipped, adhered onto a quartz lens, and the mica is removed, the resulting graphene surface replicates the flatness of the mica. Indeed, from the AFM images (Figure 5), it is clear that graphene as laid onto the SFB lens using the transfer method (panels b and c of Figure 5) is significantly smoother than graphene transferred using a conventional transfer method (Figure 5a). The root-mean-square (RMS) roughness of the double-transferred surface is 0.44 nm over $5 \mu\text{m}^2$ and 0.19 nm over $1 \mu\text{m}^2$, approaching the roughness of mica itself.⁴⁹ This is an order of magnitude less than the roughness of the non-templated surface (4.43 nm). Furthermore, the dominant features in Figure 5b, as seen from the height profile, are negative protrusions or “valleys”, enabling surfaces to come into contact during SFB measurements (Figure 2b). Low surface roughness is essential for insightful SFB experiments because the roughness essentially limits the resolution of the experiment: if the surface is rough, forces arising from liquid film structure at small surface separation will be obscured by the force required to compress surface asperities (Figure 2).

The resultant graphene surface is also free from commonly encountered polymer residue contamination because this side of graphene is never in contact with PMMA.⁵⁰ Furthermore, there is no evidence of the presence of metal nanoparticle contamination arising from incomplete etching of the copper.¹⁵ Finally, the surface is free from airborne particulates. This is because, unlike conventional transfer methods, the final graphene surface has had only brief exposure to the ambient environment. The graphene surface is protected by the mica up until the point at which it is required, and the mica is removed.

In contrast, the final surface in ordinary transfer techniques is the “top” side of the graphene, the side exposed to the air after synthesis and any polymer support.^{10–12}

Interferometry with Graphene Lenses: The gSFB. To confirm the feasibility of measuring surface forces between graphene sheets with external control of the surface potential in the gSFB, the interaction between graphene sheets across an aqueous solution of 0.1 mM KClO₄ was investigated (Figure 6; procedure detailed in the Materials and Methods). The force, as a function of surface separation in the range of ~200 nm down to 0 nm, was first measured at open circuit. At large separation, no force is detected (within the resolution of the measurement), and then very weak repulsive double-layer forces are detected in the range from tens of nanometers to the point of surface contact. The surfaces were then retracted, and a potential of -210 ± 10 mV versus the point of zero charge (see Figure S1 of the Supporting Information) was applied to both graphene surfaces. The subsequent force profile shows a large repulsive interaction, exponentially increasing with decreasing surface separation. The magnitude of force is much greater with the large applied surface potential, as expected within the standard DLVO theory. The data adheres closely to the solution of the nonlinear Poisson–Boltzmann (PB) equation for a 1:1 electrolyte between identical, charged surfaces with a sphere-on-flat geometry at -210 mV and with 0.6 mM salt concentration.⁵¹ The higher salt concentration (steeper gradient) of the PB fit compared to that expected for 0.1 mM ionic strength indicates the presence of additional ions in the double-layer region. This may result from the small 350 nA background current at this potential. This current will have an insignificant effect on the overall concentration (approximately 10 nM increase in the concentration over the duration of the experiment), but there may be an increase in the concentration at the surface where the electrochemical reaction occurs. In the absence of an applied potential, the PB fit agrees with the expected 0.1 mM ionic strength. At small separations, the fit overestimates the force compared to the measured data; the origin of this non-PB behavior is not yet clear, although we note it is also present in the electrochemical SFB measurements between gold surfaces by Kasuya and Kurihara.⁵² Crucially, upon relaxation of the surface potential (a return to open circuit), the original surface force profile was recovered, illustrating the reversibility of the system. The non-zero forces detected at open circuit potential indicate a weak charging of the graphene in the aqueous electrolyte environment, possibly because of specific adsorption.

With regard to the objective of this work, viz. demonstrating the feasibility of graphene–SFB measurements, three key points are noted: (i) The appearance of double-layer forces (and no additional repulsive force) down to nanometer separation between the two graphene sheets indicates that the surfaces are indeed sufficiently smooth, over the whole interacting area, for gSFB measurements. (ii) The strong repulsive force observed when symmetric potential is applied to the graphene surfaces indicates that the graphene sheets are continuous across the surfaces and able to support the external potential as expected. (iii) The successful use of FECO interference fringes to calculate the surface force and surface separation, with nanometer precision, demonstrates the feasibility of using the procedures outlined above for the preparation of graphene lenses and subsequent force measurement in the gSFB.

CONCLUSION

A new double-transfer procedure has been demonstrated for preparation of ultraflat graphene surfaces over macroscopic areas. This was achieved by modifying the conventional polymer transfer method with an additional transfer step using freshly cleaved mica as a perfectly clean and flat support. Graphene surfaces produced by the double-transfer procedure have a RMS roughness of less than half a nanometer (0.44 nm) over micrometer-sized areas. In comparison, surfaces produced by the conventional polymer transfer method have a RMS roughness an order of magnitude higher (4.43 nm). Furthermore, the double-transfer procedure yields graphene surfaces that are free from polymer residues commonly encountered when using conventional transfer methods.

These ultraflat graphene surfaces have been integrated into a new apparatus, the gSFB, an instrument for the measurement of surface forces and surface liquid structure at the nanoscale. We show that the graphene surfaces can be brought into clean contact and their separation and interaction force measured with subnanometer resolution by white-light interferometry. This opens up the possibility of a multitude of measurements, including graphene–graphene adhesion and friction, liquid film structure at the graphene surface, and owing to the high conductivity of graphene, potential-dependent and electrochemical effects on normal interaction forces and shear forces.

We note that the graphene transfer method reported here, the key enabling step in the process, is widely applicable for graphene and other two-dimensional (2D) material applications where macroscopic graphene sheets are required and where cleanliness and roughness are key hurdles.

ASSOCIATED CONTENT

S Supporting Information

Electrocapillary curve of CVD graphene in 0.1 mM KClO₄ (on SFB lens) (Figure S1) and unfiltered Raman spectra of graphene SFB lens, confirming the success of the transfer and demonstrating the retained quality of the few-layer graphene (Figure S2). This material is available free of charge via the Internet at <http://pubs.acs.org>.

AUTHOR INFORMATION

Corresponding Authors

*E-mail: susan.perkin@chem.ox.ac.uk.

*E-mail: nicole.grobert@materials.ox.ac.uk.

Author Contributions

[†]Jude Britton and Nico E. A. Cousens contributed equally to this work.

Notes

The authors declare no competing financial interest.

ACKNOWLEDGMENTS

The authors are grateful to the Royal Society, the European Research Council (ERC) (Starting Grant ERC-2009-StG-240500 DEDIGROWTH and Proof of Concept Grant ERC-2012-PoC 309786 DEVICE), the Engineering and Physical Sciences Research Council (EPSRC Pathways to Impact Awards), the Leverhulme Trust (F/07 134/DK and F/07 134/DN), and the John Fell Fund (Oxford University) for financial support.

■ REFERENCES

- (1) Geim, A. K.; Novoselov, K. S. The rise of graphene. *Nat. Mater.* **2007**, *6*, 183–191.
- (2) Ivaniščev, V.; Fedorov, M. V.; Lynden-Bell, R. M. Screening of ion–graphene electrode interactions by ionic liquids: The effects of liquid structure. *J. Phys. Chem. C* **2014**, *118*, 5841–5847.
- (3) Lee, C.; Li, Q.; Kalb, W.; Liu, X.-Z.; Berger, H.; Carpick, R. W.; Hone, J. Frictional characteristics of atomically thin sheets. *Science* **2010**, *328*, 76–80.
- (4) Englert, J. M.; Dotzer, C.; Yang, G.; Schmid, M.; Papp, C.; Spiecker, E.; Hauke, F.; Hirsch, A.; Gottfried, J. M.; Steinru, H.-P. Covalent bulk functionalization of graphene. *Nat. Chem.* **2011**, *3*, 279–286.
- (5) Vogel, N.; Zieleniecki, J.; Köper, I. As flat as it gets: Ultrasmooth surfaces from template-stripping procedures. *Nanoscale* **2012**, *4*, 3820–3832.
- (6) Chai, L.; Klein, J. Large area, molecularly smooth (0.2 nm rms) gold films for surface forces and other studies. *Langmuir* **2007**, *23*, 7777–7783.
- (7) Novoselov, K. S.; Geim, A. K.; Morozov, S. V.; Jiang, D.; Zhang, Y.; Dubonos, S. V.; Grigorieva, I. V.; Firsov, A. A. Electric field effect in atomically thin carbon films. *Science* **2004**, *306*, 666–669.
- (8) Ciesielski, A.; Samori, P. Graphene via sonication assisted liquid-phase exfoliation. *Chem. Soc. Rev.* **2014**, *43*, 381–398.
- (9) Vlassiuk, I.; Fulvio, P.; Meyer, H.; Lavrik, N.; Dai, S.; Datskos, P.; Smirnov, S. Large scale atmospheric pressure chemical vapor deposition of graphene. *Carbon* **2013**, *54*, 58–67.
- (10) Reina, A.; Son, H.; Jiao, L.; Fan, B.; Dresselhaus, M. S.; Liu, Z.; Kong, J. Transferring and identification of single- and few-layer graphene on arbitrary substrates. *J. Phys. Chem. C* **2008**, *112*, 17741–17744.
- (11) Li, X.; Zhu, Y.; Cai, W.; Borysiak, M.; Han, B.; Chen, D.; Piner, R. D.; Colombo, L.; Ruoff, R. S. Transfer of large-area graphene films for high-performance transparent conductive electrodes. *Nano Lett.* **2009**, *9*, 4359–4363.
- (12) Bae, S.; Kim, H.; Lee, Y.; Xu, X.; Park, J.-S.; Zheng, Y.; Balakrishnan, J.; Lei, T.; Kim, H. R.; Song, Y. I.; Kim, Y.-J.; Kim, K. S.; Ozilmez, B.; Ahn, J.-H.; Hong, B. H.; Iijima, S. Roll-to-roll production of 30-in. graphene films for transparent electrodes. *Nat. Nanotechnol.* **2010**, *5*, 574–578.
- (13) Lin, Y.-C.; Jin, C.; Lee, J.-C.; Jen, S.-F.; Suenaga, K.; Chiu, P.-W. Clean transfer of graphene for isolation and suspension. *ACS Nano* **2011**, *5*, 2362–2368.
- (14) Geringer, V.; Subramaniam, D.; Michel, A. K.; Szafranek, B.; Schall, D.; Georgi, A.; Mashoff, T.; Neumaier, D.; Liebmann, M.; Morgenstern, M. Electrical transport and low-temperature scanning tunneling microscopy of microsoldered graphene. *Appl. Phys. Lett.* **2010**, *96*, 082114.
- (15) Liang, X.; Sperling, B. A.; Calizo, I.; Cheng, G.; Hacker, C. A.; Zhang, Q.; Obeng, Y.; Yan, K.; Peng, H.; Li, Q.; Zhu, X.; Yuan, H.; Walker, A. R. H.; Liu, Z.; Peng, L.-M.; Richter, C. A. Toward clean and crackless transfer of graphene. *ACS Nano* **2011**, *5*, 9144–9153.
- (16) Chae, S. J.; Güneş, F.; Kim, K. K.; Kim, E. S.; Han, G. H.; Kim, S. M.; Shin, H.-J.; Yoon, S.-M.; Choi, J.-Y.; Park, M. H.; Yang, C. W.; Pribat, D.; Lee, Y. H. Synthesis of large-area graphene layers on polynickel substrate by chemical vapor deposition: Wrinkle formation. *Adv. Mater.* **2009**, *21*, 2328–2333.
- (17) Zhu, W.; Low, T.; Perebeinos, V.; Bol, A. A.; Zhu, Y.; Yan, H.; Tersoff, J.; Avouris, P. Structure and electronic transport in graphene wrinkles. *Nano Lett.* **2012**, *12*, 3431–3436.
- (18) Tabor, D.; Winterton, R. H. S. The direct measurement of normal and retarded van der Waals forces. *Proc. R. Soc. London, Ser. A* **1969**, *312*, 435–450.
- (19) Israelachvili, J. N. Thin film studies using multiple-beam interferometry. *J. Colloid Interface Sci.* **1973**, *44*, 259–272.
- (20) Klein, J.; Kumacheva, E. Simple liquids confined to molecularly thin layers. I. Confinement-induced liquid-to-solid phase transitions. *J. Chem. Phys.* **1998**, *108*, 6996–7009.
- (21) Pashley, R. M. DLVO and hydration forces between mica surfaces in Li^+ , Na^+ , K^+ and Cs^+ electrolyte solutions: A correlation of double-layer and hydration forces with surface cation exchange properties. *J. Colloid Interface Sci.* **1981**, *83*, 531–546.
- (22) Pashley, R. M. Hydration forces between mica surfaces in aqueous electrolyte solutions. *J. Colloid Interface Sci.* **1981**, *80*, 153–162.
- (23) Perkin, S.; Goldberg, R.; Chai, L.; Kampf, N.; Klein, J. Dynamic properties of confined hydration layers. *Faraday Discuss.* **2009**, *141*, 399–413.
- (24) Israelachvili, J. N.; Tabor, D. Measurement of van der Waals dispersion forces in the range 1.4 to 130 nm. *Nat. Phys. Sci.* **1972**, *236*, 106.
- (25) Horn, R. G.; Israelachvili, J. N. Direct measurement of structural forces between two surfaces in a nonpolar liquid. *J. Chem. Phys.* **1981**, *75*, 1400–1411.
- (26) Klein, J. Forces between mica surfaces bearing layers of adsorbed polystyrene in cyclohexane. *Nature* **1980**, *288*, 248–250.
- (27) Klein, J.; Kumacheva, E.; Mahalu, D.; Perahla, D.; Fetter, L. J. Reduction of frictional forces between solid surfaces bearing polymer brushes. *Nature* **1994**, *370*, 634–636.
- (28) Horn, R. G. Direct measurement of the force between two lipid bilayers and observation of their fusion. *Biochim. Biophys. Acta, Biomembr.* **1984**, *778*, 224–228.
- (29) Connor, J. N.; Horn, R. G. Measurement of aqueous film thickness between charged mercury and mica surfaces: A direct experimental probe of the Poisson–Boltzmann distribution. *Langmuir* **2001**, *17*, 7194–7197.
- (30) Fréchette, J.; Vanderlick, T. K. Double layer forces over large potential ranges as measured in an electrochemical surface forces apparatus. *Langmuir* **2001**, *17*, 7620–7627.
- (31) Shrestha, B. R.; Baimpos, T.; Raman, S.; Valtiner, M. Angstrom-resolved real-time dissection of electrochemically active noble metal interfaces. *ACS Nano* **2014**, *8*, 5979–5987.
- (32) Zhang, B.; Lee, W. H.; Piner, R.; Kholmanov, I.; Wu, Y.; Li, H.; Ji, H.; Ruoff, R. S. Low-temperature chemical vapor deposition growth of graphene from toluene on electropolished copper foils. *ACS Nano* **2012**, *6*, 2471–2476.
- (33) Quon, R. A.; Levins, J. M.; Vanderlick, T. K. High-precision automated measurement of surface separation for the surface force apparatus. *J. Colloid Interface Sci.* **1995**, *171*, 474–482.
- (34) Fisher, L. R.; Israelachvili, J. N. Direct experimental verification of the Kelvin equation for capillary condensation. *Nature* **1979**, *277*, 548–549.
- (35) Reina, A.; Jia, X.; Ho, J.; Nezich, D.; Son, H.; Bulovic, V.; Dresselhaus, M. S.; Kong, J. Large area, few-layer graphene films on arbitrary substrates by chemical vapor deposition. *Nano Lett.* **2009**, *9*, 30–35.
- (36) Li, X.; Cai, W.; An, J.; Kim, S.; Nah, J.; Yang, D.; Piner, R.; Velamakanni, A.; Jung, I.; Tutuc, E.; Banerjee, S. K.; Colombo, L.; Ruoff, R. S. Large-area synthesis of high-quality and uniform graphene films on copper foils. *Science* **2009**, *324*, 1312–1314.
- (37) Reina, A.; Thiele, S.; Jia, X.; Bhaviripudi, S.; Dresselhaus, M. S.; Schaefer, J. A.; Kong, J. Growth of large-area single- and bi-layer graphene by controlled carbon precipitation on polycrystalline Ni surfaces. *Nano Res.* **2010**, *2*, 509–516.
- (38) Zhou, H.; Yu, W. J.; Liu, L.; Cheng, R.; Chen, Y.; Huang, X.; Liu, Y.; Wang, Y.; Huang, Y.; Duan, X. Chemical vapour deposition growth of large single crystals of monolayer and bilayer graphene. *Nat. Commun.* **2013**, *4*, 2096.
- (39) Li, X.; Magnusson, C. W.; Venugopal, A.; Tromp, R. M.; Hannon, J. B.; Vogel, E. M.; Colombo, L.; Ruoff, R. S. Large-area graphene single crystals grown by low-pressure chemical vapor deposition of methane on copper. *J. Am. Chem. Soc.* **2011**, *133*, 2816–2819.
- (40) Liu, W.; Kraemer, S.; Sarkar, D.; Li, H.; Ajayan, P. M.; Banerjee, K. Controllable and rapid synthesis of high-quality and large-area Bernal stacked bilayer graphene using chemical vapor deposition. *Chem. Mater.* **2014**, *26*, 907–915.

- (41) Bhaviripudi, S.; Jia, X.; Dresselhaus, M. S.; Kong, J. Role of kinetic factors in chemical vapor deposition synthesis of uniform large area graphene using copper catalyst. *Nano Lett.* **2010**, *10*, 4128–4133.
- (42) Murdock, A. T.; Koos, A.; Britton, T. B.; Houben, L.; Batten, T.; Zhang, T.; Wilkinson, A. J.; Dunin-Borkowski, R. E.; Lekka, C. E.; Grobert, N. Controlling the orientation, edge geometry, and thickness of chemical vapor deposition graphene. *ACS Nano* **2013**, *7*, 1351–1359.
- (43) Ferrari, A. C.; Meyer, J. C.; Scardaci, V.; Casiraghi, C.; Lazzeri, M.; Mauri, F.; Piscanec, S.; Jiang, D.; Novoselov, K. S.; Roth, S.; Geim, A. K. Raman spectrum of graphene and graphene layers. *Phys. Rev. Lett.* **2006**, *97*, 1–4.
- (44) Ferrari, A. C. Raman spectroscopy of graphene and graphite: Disorder, electron–phonon coupling, doping and nonadiabatic effects. *Solid State Commun.* **2007**, *143*, 47–57.
- (45) Graf, D.; Molitor, F.; Ensslin, K.; Stampfer, C.; Jungen, A.; Hierold, C.; Wirtz, L. Spatially resolved Raman spectroscopy of single- and few-layer graphene. *Nano Lett.* **2007**, *7*, 238–242.
- (46) Dresselhaus, M. S.; Jorio, A.; Hofmann, M.; Dresselhaus, G.; Saito, R. Perspectives on carbon nanotubes and graphene Raman spectroscopy. *Nano Lett.* **2010**, *10*, 751–758.
- (47) Chen, S.; Cai, W.; Piner, R. D.; Suk, J. W.; Wu, Y.; Ren, Y.; Kang, J.; Ruoff, R. S. Synthesis and characterization of large-area graphene and graphite films on commercial Cu–Ni alloy foils. *Nano Lett.* **2011**, *11*, 3519–3525.
- (48) Rafiee, J.; Mi, X.; Gullapalli, H.; Thomas, A. V.; Yavari, F.; Shi, Y.; Ajayan, P.M.; Koratkar, N. A. Wetting transparency of graphene. *Nat. Mater.* **2012**, *11*, 217–222.
- (49) Senden, T. J.; Ducker, W. A. Surface roughness of plasma-treated mica. *Langmuir* **1992**, *8*, 733–735.
- (50) Ishigami, M.; Chen, J. H.; Cullen, W. G.; Fuhrer, M. S.; Williams, E. D. Atomic structure of graphene on SiO₂. *Nano Lett.* **2007**, *7*, 1643–1648.
- (51) Chan, D. Y. C.; Pashley, R. M.; White, L. R. A simple algorithm for the calculation of the electrostatic repulsion between identical charged surfaces in electrolyte. *J. Colloid Interface Sci.* **1980**, *77*, 283–285.
- (52) Kasuya, M.; Kurihara, K. Characterization of ferrocene modified electrode using electrochemical surface forces apparatus. *Langmuir* **2014**, *30*, 7093–7097.